論文 / 著書情報
Article / Book Information

Title	Centrifuge study on the effect of the SCP improvement geometry on the mitigation of liquefaction-induced embankment settlement
Authors	Yang Li, Masaki Kitazume, Akihiro Takahashi, Kenji Harada, Jun Ohbayashi
Citation	Soil Dynamics and Earthquake Engineering, Vol. 148, 106852
Pub. date	2021, 9
DOI	http://dx.doi.org/10.1016/j.soildyn.2021.106852
Creative Commons	See next page.
Note	This file is author (final) version.

License

Title:

Centrifuge study on the effect of the SCP improvement geometry on the mitigation of liquefaction-induced embankment settlement

Authors:

Yang Li
Department of Civil and Environment Engineering, Tokyo Institute of Technology, Japan
2-12-1 Ookayama, Meguro-Ku, 152-8552 Tokyo, Japan
E-mail address: ri.y.ac@m.titech.ac.jp

Masaki Kitazume
Department of Civil and Environment Engineering, Tokyo Institute of Technology, Japan
2-12-1 Ookayama, Meguro-Ku, 152-8552 Tokyo, Japan
E-mail address: kitazume.m.aa@m.titech.ac.jp

Akihiro Takahashi
Department of Civil and Environment Engineering, Tokyo Institute of Technology, Japan
2-12-1 Ookayama, Meguro-Ku, 152-8552 Tokyo, Japan
E-mail address: takahashi.a.al@m.titech.ac.jp

Kenji Harada
Geo-Technical Division, Fudo Tetra Corporation, Japan
7-2, Nihonbashi-Koami-chou, Chuou-ku, Tokyo 103-0016, Japan
E-mail address: kenji.harada@fudotetra.co.jp

Jun Ohbayashi
Geo-Technical Division, Fudo Tetra Corporation, Japan
7-2, Nihonbashi-Koami-chou, Chuou-ku, Tokyo 103-0016, Japan
E-mail address: jun.ohbayashi@fudotetra.co.jp

Soil Dynamics and Earthquake Engineering, 148, 106852, 2021
Official URL: https://doi.org/10.1016/j.soildyn.2021.106852

Keywords:
liquefaction countermeasure, sand compaction pile, improvement geometry, centrifuge test

Abstract:

Liquefaction of foundation soil causes significant damage to infrastructures. The sand compaction pile (SCP) method is a countermeasure against liquefaction to densify the ground by installing dense sand piles. In recent years, an innovative method has been developed to install sand piles into the ground at any angle. In this study, a series of dynamic centrifuge tests are carried out to investigate the effects of the angle of the SCP improvement zone on mitigating the liquefaction-induced settlement of embankment crests. The lateral displacement beneath the embankment toes is mitigated by the presence of the improvement zone installed in the foundation ground. In particular, the case with a 50° improvement zone is the most effective in mitigating lateral displacement and contributes to the lower settlement of the embankment.

1. Introduction

During an earthquake, saturated loose sandy soil is characterized by a substantial rise in excess pore water pressure, leading to a drastic loss of its strength and stiffness. When the excess pore water pressure reaches the initial effective overburden stress, soil particles do not support each other, and liquefaction takes place, which usually causes severe damage, such as cracking, slumping, lateral spreading and settlement, to river dykes, levees and road embankments. For instance, many embankments and river dykes that failed due to the liquefaction of foundation ground were reported during the 1964 Alaskan and Niigata earthquake [1], [2], the 1983 Nipponkai-Chubu, Japan earthquake [3], and the 1995 Hyogoken-Nambu, Japan earthquake [4], among many others. During the 2011 Great East Japan earthquake, more than 2000 locations of embankments suffered some level of damage caused by liquefaction of the foundation ground [5]. Soil liquefaction and related damage to earthen structures have been extensively studied by many researchers in past decades [6]–[10]. It was reported that the primary cause of embankment settlement was the lateral deformation of liquefied soil beneath the embankment away from the embankment center.

To date, many liquefaction countermeasures based on various principles have been developed (e.g., densification, deep mixing, drainage). Among them, the SCP method is a typical ground densification method, which has often been applied to mitigate liquefaction to densify the ground by installing vertical compacted sand piles into the ground. The SCP method is considered to increase ground density and uniformity [11]. The effectiveness of the SCP method as a countermeasure against liquefaction has been confirmed in past earthquakes, including the 1978 Miyagi-Oki earthquake [12], showing that this method is one of the most reliable ground improvement methods in Japan [13]. It is also expected to be applied to the ground improvement of civil engineering structures in the future.

On the other hand, there are numerous existing soil structures worldwide that were either constructed before the seismic design standard was established or without it [14]. To prevent potential damage to these existing structures from liquefaction in future earthquakes, it may be necessary to remediate the foundation soil. However, the conventional SCP method constructing sand piles in the vertical direction is not able to densify ground underneath an existing structure. As mentioned above, during earthquake loading, most of the structural settlements and deformations are caused by the lateral movement of liquefied soils under the structure. To apply the SCP method to existing embankment structures, countermeasures are designed to provide confinement to the liquefied foundation soils moving away from the embankment centerline toward the free field, for which well-compacted sand piles are constructed under embankment toes in current practice. It has been reported that the occurrence of excessive settlement associated with large lateral deformation of liquefied foundation soils could be prevented effectively by this method; however, some embankment crest settlement was inevitable due to the deformation of liquefied sand under the embankment and volumetric strain with excess pore pressure dissipation under the embankment [15]–[18].

With advancements in machinery, a new type of SCP method has been recently developed, the SAVE-SP method, which enables the vertical installation of sand piles or the installation of sand piles at a specific angle into the ground. As the machine for this method is small, compacted sand piles can be formed in any direction underneath a structure, which is expected to prevent liquefaction and associated settlement more effectively [19], [20]. In addition, in previous studies, Yoshida et al. [21] performed shaking table tests where wooden sticks instead of sand piles were installed into the loose sand layer under residential houses at vertical and inclined angles. It was found that the wooden sticks installed at an inclined angle were more effective than those installed at a vertical angle. Rasouli et al. [22], [23] conducted 1 g model tests to evaluate the effect of sheet-pile walls as a countermeasure around the building's foundation and that combined with installing inclined drains under the structure. It was observed that the settlement and tilting of the building are reduced significantly in combination with inclined drains under the structure due to the installation of drains providing an area of nonliquefied ground under the building edges.

The geometric form of the improvement zones may affect the response and deformation behavior of the improved ground. However, these influences are not well investigated and incorporated into the current design precisely. The reliable and performance-based design of the new SCP method for embankments requires a clear understanding of the effect of various parameters that influence performance. In this study, four dynamic centrifuge experiments are carried out to investigate the effects of the angle of the SCP improvement zones on the liquefaction-induced deformation and response of the ground.

2. Centrifuge test program

A series of dynamic centrifuge tests are conducted to evaluate the effectiveness of SCP-improved ground with various geometric improvement forms and to investigate the effects of the geometry of the improved zone on the ground response and deformation mechanism of embankments and foundation ground. In the centrifuge test program, the focus is on the angle of the improvement zone, which is defined as the angle between the SCP improvement form and the ground base, in which the angle is changed from 50 to 90 degrees. Dynamic centrifuge tests are carried out utilizing the Tokyo Tech Mark III centrifuge facility [24] with a radius of 2.45 m at a centrifugal acceleration of 50 g. The model configurations and the entire test results are presented in prototype scale units unless indicated otherwise.

2.1 Design and description of centrifuge models

Four dynamic centrifuge tests are conducted on three different angles of the improvement zone over 50 to 90 degrees, as well as the benchmark model without any improvement. The model configurations are shown in Fig. 1 and Table 1. All tests simulate a prototype soil deposit of 7.5 m depth and an embankment of 2.5 m height with a 1:2 slope. Case 1 constitutes the benchmark model under the typical condition that an embankment is supported by saturated loose sandy ground without any ground improvement. In Case 2, the vertical SCP improvement zones are placed under the embankment toes, which represents a conventional liquefaction remediation design for the existing embankment. Cases 3 and 4 simulate the improved ground using the new type of SCP method, where the densified improvement zones are constructed at the angles of 60 and 50 degrees within the foundation ground. It should be noted here that the SCP improvement zone modeled in this study is not the same as the real condition of SCP improved ground. As shown in Fig. 2(a), in the practical design of SCP-improved ground, the interval of SCPs is determined based on the targeted density of the ground, and the extent of SCP improvement will be determined to ensure the stability of the embankment [25]. In practice, the SCP improvement zone is considered a composite ground consisting of dense SCPs and adjacent soil densified by SCPs. In this study, the SCP improvement zone is modeled by a uniform sand block with a relative density Dr = 90% for easy model preparation. To determine the extent of the SCP improvement zone in the centrifuge experiment, preliminary experiments were conducted. Since this study focuses on the effect of the angle of SCP on mitigating embankment settlement, the extent of the SCP improvement zone is set to be large (5 m at the proto scale) so that the obvious effect can be confirmed.

2.2 Model preparation

A rigid container with inner dimensions of 600×150×400 mm is used in the tests. The front of the rigid container has a transparent window, which enables observation of the model ground in the container during the experiment. Toyoura sand is used in the tests for the foundation and the improvement zone, whose properties are shown in Table 2.

In Case 1, the uniform sand ground is made by the air pluviation method to the relative density, Dr ≈ 50%. The sand is poured through the air from a hopper, while the falling height is kept constant to obtain the desired relative density. In Cases 2, 3, and 4, the SCP improvement zones are made by tamping with 10% water content to Dr ≈ 90% first and then freezing. The front window of the container is disassembled, and the frozen soil blocks are placed at predetermined positions, as shown in Fig. 3. The remaining unimproved portions are filled with sand by air pluviation to the relative density, Dr ≈ 50%. DL clay, which consists of 90% silt and 10% clay, is mixed with 22% silicon oil by weight to build the embankments, having a unit weight of 18 kN/m^3. After the foundation ground is constructed, the embankment is carefully placed on the foundation ground at the desired place. The model ground is saturated with a mixture of water and 2% Metolose (hydroxypropyl methylcellulose) by weight of water to achieve a viscosity of approximately 50 times the viscosity of water. The purpose of using Metolose solution is to ensure the compatibility of the prototype permeability of the soil and to set up the affinity between dynamic and diffusion scaling laws [26]. The deaired Metolose solution is dripped slowly from the top of the container to the ground surface under vacuum conditions, which is continued until the water table reaches the top surface of the foundation ground. This saturation process requires approximately 48 hours.

Accelerometers and pore pressure transducers are installed as shown in Fig. 1 during the model preparation. They are installed to measure the accelerations and excess pore water pressure (△u) at three regions representing different stress states: (1) free field, defined as the region that is unaffected by the embankment load; (2) under the embankment toe where static shear stress exists; and (3) under the center of the embankment where large effective stress exists. Potentiometers are set at the embankment crest to measure the crest settlement during the experiment, and a laser displacement transducer is placed at the embankment toe to measure the horizontal displacement of the embankment toe. The spaghetti noodle sticks are installed at predetermined positions between the foundation ground and the glass window of the container. After model saturation, the noodles become soft and act as markers that are used to map deformation patterns and magnitudes within the foundation ground.

2.3 Centrifuge test description

All the models are subjected to sinusoidal waves two times with a dominant frequency of 1 Hz, where the acceleration amplitude of the first shaking is approximately 150 gal and that of the second shaking is approximately 220 gal. Fig. 4 shows the acceleration time histories of input base motions for Case 1 and Arias intensities of input base shakings for all cases for comparison. It is recognized from Fig. 4 that there is no noticeable difference in input motions between each case. The second shaking is imparted after full dissipation of pore water pressure in the foundation ground. Table 1 summarizes the model ground conditions and the peak acceleration of input motions in each case. After completion of the tests, each model is carefully inspected to measure the final locations of noodles for mapping the deformed shape.

3. Test results and discussion

3.1 Excess pore water pressure and settlement responses

Figures 5-8 present time histories of the excess pore water pressures and settlements of the embankment crest for four cases during the first and second shakings. All the test results shown in the following sections are on the prototype scale unless mentioned otherwise. The excess pore water pressure (EPWP) is measured at several representative locations, as shown in Fig. 1. The evolution of EPWP plays a vital role in the understanding of liquefaction phenomena. The initial effective vertical stress at the relevant location is plotted with a horizontal dashed line in the figures (r_u = 1 line). The initial vertical effective stresses due to embankment loading are calculated based on the influence values assuming the foundation ground to be elastic semi-infinite, as proposed by Osterberg [27]. Soils at a certain depth undergo liquefaction if the excess pore water pressure reaches the initial vertical effective stress (r_u = 1 line). The ends of the shakings are indicated with vertical dashed lines in the figures.

The EPWP time histories during the first shaking event of A_{max} ≈ 150 gal are presented in Fig. 5. In the free field of the benchmark model (Case 1), the EPWP at W6 (at a depth of 2.0 m) attains the initial effective vertical stress indicated by the r_u=1 line at 25 s after the base shaking starts and that at W3 (at a depth of 5.5 m) reaches the r_u=1 line at 30 s, corresponding to the condition of sand liquefaction at these regions. These results demonstrate that the liquefaction of the sand layer in the free field starts near the ground surface and propagates downward. Under the embankment toe, the EPWP at W5 reaches the r_u = 1 line at almost the same time with the same depth in the free field (W6). Unfortunately, the pore water pressure transducer W2 did not work correctly because of the EPWP beyond the measurable range from 25 s to 90 s, but it is presumed from measured data that the EPWP at W2 also reaches the r_u=1 line at approximately 30 s, which means that liquefaction also occurred under the embankment toes during the first shaking in Case 1. Beneath the embankment center, a low EPWP is observed at a depth of 2.0 m (W4), with a significant reduction in EPWP during shaking (from approximately 25 s). The EPWP at the deeper portion under the center of the embankment (W1) is generated to the same value as that in the free field at the same depth (W3), but the EPWP does not reach the r_u=1 line. Such lower EPWP values beneath the embankment were also reported by other centrifuge and 1 g tests [9], [15], [28].

The deviatoric stress induced by the embankment surcharge is a beneficial component that prevents the buildup of EPWP during shaking. Furthermore, the rapid liquefaction in the free field might have reduced the confinement (horizontal effective stress) of the soil below the embankment, leading to the soil below the embankment tending to move laterally away due to large induced shear stress. This mechanism dictates the soil dilation, resulting in a reduction in the EPWP. In addition, some RPI researchers have reported that drainage is more significant in the sand layer under higher confining pressure[29]–[31]. The SCP improvement zone is considered to provide higher confinement of the soil under the embankment. Therefore, it may enhance the faster drainage of the soil under the embankment.

In Case 2, improved by 90° improvement zones blow the embankment toes; unfortunately, the pore water pressure transducers W3 and W6 indicated that the EPWP in the free field did not work correctly from 25 s because of the EPWP was beyond the measurable range. However, it is presumed from the measured data that the situation of the free field in Case 2 is similar to Case 1 in terms of liquefaction that occurred in those regions. At W5 beneath the embankment toe, similar EPWP behavior is observed to that in Case 1, which indicates that liquefaction also occurs below the embankment toes in Case 2. Unfortunately, the pore water pressure transducer W2 in Case 2 did not work because of some unforeseen reasons and hence is not shown in Fig. 5. Under the embankment centerline, the EPWP at the deeper portion (W1) is very similar to that in Case 1. However, different behavior is observed at the shallower portion beneath the embankment center (W4) between Case 2 and Case 1. There is no reduction in EPWP at W4 in Case 2 during the first shaking. This may be attributed to the smaller horizontal deformation beneath the embankment center due to the confinement of the improvement zones.

On the other hand, quite different responses of EPWP are observed in Case 3 and Case 4 during the first shaking compared to the above two cases. In Case 3, which has inclined improvement zones with 60° angles under the embankment, even though there is no significant difference in the input acceleration between each case (see Fig. 4(b)), the EPWP at W6 in the free field is generated fast at the beginning of shaking but decreases immediately, although shaking continues. Similar EPWP responses are also observed at the deeper portion in the free field (W3), below the embankment toe (W2 and W5) and under the embankment center (W1 and W4). This EPWP response is not clear, but one possible reason is that the pore pressures propagate to the improvement zones very quickly due to the large pressure difference between the improvement zone and surrounding sand. In Case 4, the EPWP at W6 is observed to be similar to that in Case 1 during shaking, which indicates that liquefaction occurred in the free field near the ground surface. Unfortunately, W3 did not work correctly from 25 s. Under the embankment toe, at W5, the EPWP starts to increase at the beginning of shaking but decreases immediately, as observed in Case 3. However, at W2, a high EPWP is generated, which reaches the r_u=1 line but dissipates immediately during shaking. The EPWP under the embankment center in Case 4 is very similar to that observed in Case 3.

Settlements measured at the embankment crest (P1, shown in Fig. 1) during the first shaking are shown in Fig. 6. In the benchmark model Case 1, the settlement begins with the EPWP increasing within the foundation ground (10-25 s) and increases rapidly when liquefaction occurs below the embankment toe and in the free field from 25 s (see Fig. 5). A relatively large embankment crest settlement of approximately 0.38 m is measured. Essentially, almost all of this settlement takes place during shaking. The settlement response in Case 2 is very similar to that in Case 1 until 35 s during shaking due to the similar EPWP responses in Cases 1 and 2. In contrast, the settlement rate is decreased from 35 s during shaking, which is considered due to the effectiveness of the vertical improvement zones under the embankment toes for mitigating the lateral displacement of the ground below the embankment, which will be discussed in Subsection 3.3. On the other hand, a significantly small amount of settlements is observed in Cases 3 and 4. Because of the significantly lower EPWP values below the embankment in these two cases, the stiffness of the ground below the embankment in Cases 3 and 4 does not degrade significantly during the first shaking. It is expected that the free field response is not influenced by the embankment and the boundary effect of the container side. However, the space of the container used in this study is limited. Then, some influence from the embankment and container side on the free field response was unavoidable because a sufficient distance could not be secured. As Fig. 5 shows, the EPWPs generated under the embankment in Cases 3 and 4 are very low compared to those in Cases 1 and 2. The author believes that even though the EPWP responses in the free field in Cases 3 and 4 become similar to those in Cases 1 and 2, and the settlement result does not change much during the first shaking. For the sake of brevity, it is not shown in this paper, but the sensitivity analysis by finite element analysis showed that the EPWP response in the free field could be different depending on the container width, while its impact on the deformation of the foundation ground under the embankment was not significant.

Figure 6 shows the EPWP time histories during the second shaking event of $A_{max} \approx 220$ gal. The responses of EPWP in Case 1 and Case 2 are almost the same as those during the first shaking, i.e., liquefaction occurs below the embankment toe and in the free field, whereas the soil under the center of the embankment does not reach a liquefaction state, but high EPWP is generated at the deeper portion. During the second shaking, in Cases 3 and 4, liquefaction occurs below the embankment toe and in the free field, caused by the large cyclic shear stress induced by the larger shaking. It is worth noting that the EPWPs at the deeper portion under the center of the embankment in Cases 3 and 4 seem to be larger than those in Cases 1 and 2. However, the EPWP values at the shallower portion (at W4) in Cases 3 and 4 are smaller than those in Cases 1 and 2. This may be because the deeper portion is liquefied during the shaking period and prevents the waves from propagating upward. Regarding the higher excess pore water pressure generated under the embankment in the improved ground, similar behavior was also observed in other centrifuge experiments and numerical analyses [17], [18], [32], where the ground under the embankment toes improved by SCPs as well as the deep mixing method and sheet pile. The higher excess pore water pressure may be partly due to the horizontal deformation suppressed by the SCP improvement zone, resulting in the soils under the embankment showing a contractive response (i.e., generation of EPWP).

Figure 7 depicts the settlement time histories of the embankment crest during the second shaking. Herein, it should be noted that the ground conditions of the cases are altered due to the first shaking. Particularly, in Case 1 and Case 2, the density of the soil below the embankment should have become denser than that before being subjected to the first shaking because of considerable settlement during the first shaking. Additionally, the gradients of the embankment slope in Case 1 and Case 2 are less than those before the first shaking, which indicates a reduction in shear stress within the ground induced by the embankment. In Case 1, excessive settlement is also observed during the second shaking. In Case 2, the settlement starts at a lower rate in comparison with Case 1, when liquefaction occurs within the ground. In Cases 3 and 4, less settlement is observed in comparison with Case 1, and settlement ceases faster in Case 4 compared to Case 3, which suggests that a 50° improvement (Case 4) is more effective in mitigating the embankment settlement in comparison with a 60° improvement (Case 3).

There are two types of ground deformation that contribute to liquefaction ground settlement: shear deformation and volumetric change [33]. Figs. 6 and 8 show that most of the settlements occurred during shaking and that those after shaking were very small, which indicates that volumetric change due to drainage occurred during shaking. The average volumetric strains of the ground under the embankment in each case after shaking were confirmed by the measured volume change under the embankment. In addition, 1% to 2.5% of the volumetric strains were found within the ground under the embankment. The following effects of these volumetric strains on the behavior of excess pore water pressure and settlement are considered. One is that the amount of settlement due to drainage is approximately 1% to 2.5%, including the amount of settlement during shaking. Therefore, compared with the completely undrained condition, the result of the settlement presented here is slightly overestimated. Another is that if the ground is under completely undrained conditions, the excess pore water pressure may be generated faster than that under drained conditions. As a result, it is possible that the amount of settlement due to shear deformation of the ground will be larger.

3.2 Distribution of maximum excess pore pressures under the embankment

Figures 8 and 9 illustrate the distribution of the maximum EPWP with depth under the embankment center and toe subjected to the first and second shakings, respectively. It should be noted that the maximum EPWP values indicated in Figs. 8 and 9 are the monotonic components picked up from the EPWP time histories. The dashed lines in the figure represent the initial vertical effective stress with depth. These figures are plotted to clarify the extent of liquefaction in different cases during each shaking event. In the first shaking, as shown in Fig. 9, the maximum EPWP values do not reach the initial vertical effective stress under the embankment center in all cases, which means that the soil under the embankment centerline is not liquefied even though the values of the maximum EPWP are different between each case. The effect of the improvement angle on the EPWP values will be discussed later using Fig. 11. Beneath the embankment toe, at a depth of 2.0 m, the maximum EPWP in Case 1 and Case 2 reaches the initial effective stress, indicating that liquefaction occurs beneath the toes in these two cases. At the same location, the maximum EPWP values in Cases 3 and 4 are below the initial effective stress line, indicating that the soil is not liquefied beneath the toes in these two cases during the first shaking.

Figure 9 shows the maximum EPWP distribution for all cases during the second shaking event (Amax≈220 gal). Under the embankment center, the maximum EPWP at the deeper portion (at a depth of 5.5 m) tends to be a similar value in all cases, among which the improved ground cases (i.e., Case 2, Case 3, and Case 4) showed higher EPWPs than the unimproved ground case. At the shallower portion (at a depth of 2.0 m), the EPWPs in all cases stay at much lower values than the initial effective stress. Beneath the embankment toe, the soils are considered liquefied irrespective of the ground conditions because the EPWPs in all cases at this location reach the initial effective stress.

As mentioned that the EPWP plays a vital role in the liquefaction phenomena and related effects, it is motivated to evaluate the effect of the angle of improvement zone on the generation of EPWP within the ground. To achieve this, Fig. 11 depicts the relationship between the angle of the improvement zone and the maximum EPWP at the representative locations within the ground subjected to the first and second shakings.

During the first shaking event (see Fig. 11(a)), the response in the free field seems almost the same irrespective of the angle of the improvement, since the values have no variation along the angle of the improvement zone. Beneath the embankment toe, the maximum EPWPs generated in the cases with 50 and 60 degree improvement zones are smaller than those in the cases without improvement and with 90 degree improvement zones. The same trend is also observed beneath the embankment center (see the black lines in Fig. 11(a)), especially at the deeper portion below the embankment center, where the EPWP values measured in Cases 3 and 4 are approximately 20% of the values measured in Cases 1 and 2. Overall, during the first shaking with a relatively smaller acceleration amplitude, a lower EPWP is observed in Cases 3 and 4 than in Cases 1 and

2, except in the free field.

The results of each case for the second shaking are shown in Fig. 11(b). In the free field, it seems that there is no relation to the angle of the improvement. A similar trend is observed beneath the toe. In other words, there is no significant influence of the degree of improvement zone on the maximum EPWP in the free field and beneath the toe. However, under the embankment center, the maximum EPWP at a deeper portion (at a depth of 5.5 m) is larger in the improvement cases, especially in Cases 3 and 4. This trend is the opposite of the situation in the first shaking. At the shallower portion beneath the embankment center, the maximum EPWP generated in Cases 3 and 4 is smaller than that in Cases 1 and 2, which is the same trend as that in the first shaking.

3.3 Lateral displacement beneath embankment toe

As mentioned in the introduction, the major cause of the embankment settlement induced by liquefaction of the foundation ground is the lateral displacement of liquefied soil beneath the embankment away from the embankment center. Countermeasures in the remediation program for embankments, therefore, aim at mitigating crest settlement by providing confinement to the liquefiable foundation soils by forming remediated stiff zones in the liquefiable soil layer under embankment toes. To evaluate the effectiveness of the improvement zone with a different angle, the lateral displacement beneath the embankment toe is discussed in this subsection.

Fig. 12 depicts the lateral displacement distribution beneath the embankment toe after the first and second shakings. In Fig. 12, the dashed lines present the results after the first shaking, and the solid lines present those after the second shaking. It should be noted that the displacement distributions after the second shaking contain the displacement produced during the first shaking.

After the first shaking, the lateral displacement in Case 1 is observed with a maximum value of approximately 0.2 m at a depth of 2.0 m and decreases toward the ground surface and base. In Case 2, the shape of lateral displacement distribution beneath the toe is similar to Case 1, but the amount of displacement was mitigated compared to that in Case 1 below a depth of 1.5 m. In Case 3 and Case 4, the lateral displacements are significantly smaller than the other two cases, which is attributed to the lower EPWP generation during the first shaking (see Figs. 5 and 9).

After the second shaking, a significant increment of lateral displacement is observed in Case 1 at the whole depth, especially at depths from 1.0 to 3.5 m. This might be because the EPWP remains lower at the shallower portion beneath the center of the embankment (see Figs. 9 and 10), and then the soil in that portion does not lose the strength and stiffness significantly. Whereas, the EPWP at the deeper portion is high. Then, a large lateral displacement of sand can be expected below the portion where EPWP remains lower beneath the embankment. A similar deformation mechanism was also reported in other studies [34]–[36]. The lateral displacement in Case 2 also increases during the second shaking due to liquefaction occurring again beneath the toe and in the free field (see Fig. 7), but the amount is smaller than that in Case 1. In Cases 3 and 4, the increment of lateral displacements is observed after the second shaking, caused by liquefaction that occurred during the second shaking. Although a high EPWP is generated at the deeper portion below the embankment during the second shaking (see Fig. 10), the lateral displacement at the deeper portion seems mitigated more effectively in Cases 3 and 4 than in the cases without improvement and with a 90 degree improvement zone.

From the above results, it is suggested that the main mechanism responsible for the settlement of the embankment is the form of soil softening due to a decrease in effective stresses (generation of EPWP) in the foundation ground, permitting vertical compression to accompany lateral displacement. In this study, the ground improved by 50° angle improvement zones is the most effective for mitigating the lateral displacement.

To evaluate the effect of different improvement angles on mitigating lateral displacement quantitatively, the area of the lateral displacement distribution along the depth (i.e., the amount of laterally deformed soil) is calculated from the distribution shown in Fig. 12. Fig. 13 presents the relationship between the angle of the SCP improvement zone and the area of lateral displacement. During the first shaking, the overall lateral displacement in Cases 3 and 4 is significantly smaller than that in Cases 1 and 2 due to the much lower EPWP generated in Cases 3 and 4 compared to the other two cases (see Fig. 11(a)). During the second shaking, in all cases, the amount of total lateral displacement is more than that after the first shaking. This might be due to the liquefaction state sustaining a longer time than the first shaking (see Figs. 5 and 7). Overall, Fig. 13 confirms the effectiveness of the inclined improvement zone in mitigating lateral displacement. Among them, the improvement with the 50° angle case shows the best performance.

3.4 Settlement beneath the embankment

As mentioned in section 3.1, some extent of drainage under the embankment might occur during shaking, even though undrained conditions are aimed at in the model test. According to the measured volume change under the embankment, the drainage effect on the ground settlement is small. Several centrifuge tests (e.g., [15]) and shaking table tests at 1 g (e.g., [37]) have been conducted to explore the effectiveness of remedial countermeasures beneath embankment toes for reducing crest settlement. The above-referenced studies showed that embankment crest settlement after shaking was greater than half of the settlement in the case without countermeasures, although the lateral displacements beneath the toes were significantly mitigated with a countermeasure. One reason for this is that the embankment settlement contains the shaking-induced compression of the embankment itself. To eliminate this component from the embankment settlement, a comparison of the settlement below the embankment is also useful.

Figure 14 depicts the settlement distribution at the embankment bottom after the first and second shakings. In Fig. 14, the dashed lines present the results after the first shaking, and the solid lines present the results after the second shaking. In Case 1, the bottom of the embankment is settled overall, where the largest settlement occurred under the crest and decreased toward the toe for both the first and second shakings. In Case 2, the difference compared to Case 1 is that the soil shows an upward heave near the toe. It might be that the lateral displacement constraint is imposed by the vertical improvement zone, resulting in formations of a low strength exit path near the toes where liquefaction occurred (see Figs. 9 and 10). This deformation pattern would lead to an increase in the settlement under the crest. The same observation was also reported by the other centrifuge tests (e.g., [16], [22]). In Case 3, the soil beneath the toe also heaves but is smaller than that in Case 2. In Case 4, no significant heave deformation near the toe is observed. This might be due to the presence of stiff improvement zones below the toes, and the volume of the deformable soil below the toes decreases. This effect should be significant in Case 4, as there is a larger improvement area below the toes.

3.5 Settlement of embankment crest

Figure 15 plots the vertical displacement of the embankment crest (P1 shown in Fig. 1) against the angle of the improvement zone immediately after the first and second shakings, as well as the settlement due to the dissipation of EPWP after shaking. In every shaking event, the difference between settlement immediately after shaking and that after dissipation of EPWP is very small, which demonstrates that the main settlement occurs during shaking.

In Fig. 15, the shape of the lines is very similar to that shown in Fig. 13, which indicates that the relationship between the angle of the improvement zone and the area of lateral displacement has a one-to-one relationship. It is verified that there is a strong correlation between the lateral displacement beneath the toes and the settlement of the embankment. Additionally, it is suggested that the improvement conditions that can mitigate lateral displacement more effectively are also effective in mitigating embankment settlement. It is clear from Fig. 15 that all improvement cases show the effectiveness of mitigating embankment crest settlement. Among them, Case 4 improved by a 50° angle is the most effective in mitigating the settlement, which is considered to be because the lateral displacement beneath the toes is most mitigated in comparison with other cases.

4. Conclusions

A series of dynamic centrifuge tests are carried out to investigate the effects of the angle of the SCP improvement zone on mitigating the liquefaction-induced settlement of embankment crests. The following major conclusions are drawn from the test results:

(1) The excess pore water pressure (EPWP) responses in the ground are influenced by the angle of the improvement zone. During small shaking (150 gal), the maximum EPWP under the

embankment center and near the toe in the case of the 60° and 50° improvement zones is less than that in the unimprovement case and 90° improvement case. During the larger shaking (220 gal), the maximum EPWP under the embankment center at the deep layer tends to become higher values in the 60° and 50° improvement zones in comparison with the unimprovement case and 90° improvement case. At a shallower portion of the foundation ground under the embankment center, the trend of the maximum EPWP is similar to that during small shaking, but there is a marginal difference between cases under the toe.

(2) It is confirmed that the lateral displacement beneath the embankment toes is mitigated by the presence of the improvement zone installed in the foundation ground. In particular, the case with a 50° improvement zone is the most effective and contributes to the lower settlement of the embankment.

(3) The deformation pattern of the soil below the embankment toe is also important for the mitigation of crest settlement. In the case with the 90° improvement zone, a relatively larger heave is observed beneath the embankment toe, whereas in the 60° and 50° improvement cases, such heave deformation near the toe is suppressed. Since this heave deformation beneath the toe makes the crest settlement larger, it is suggested that in addition to lateral displacement beneath the embankment toe, the deformability of the soil under the embankment toe is also important for mitigating the crest settlement of the embankment.

References

[1] D. McCulloch and M. Bonilla, "Railroad damage in the Alaska Earthquake," *J. Soil Mech. Found. Div.*, vol. 93, no. SM5, pp. 89–100, 1967, [Online]. Available: http://trid.trb.org/view.aspx?id=126871.

[2] F. Kawakami and A. Asada, "Damage to the ground and earth structures by the Niigata earthquake of June 16, 1964," *soils Found.*, vol. 6, no. 1, pp. 14–30, 1966, doi: 10.1248/cpb.37.3229.

[3] S. Tani, "Consideration of Earthquake Damage to Earth Dam for Irrigation in Japan," in *Proceedings of the 2nd International Conference on Recent Advances in Geotechnical Earthquake Engineering and Soil Dynamics*, 1991, pp. 1137–1142.

[4] S. Tani, "Damage to earth dams," *Soils Found.*, vol. Special, pp. 263–272, 1996.

[5] F. Oka, P. Tsai, S. Kimoto, and R. Kato, "Damage patterns of river embankments due to the 2011 off the Pacific Coast of Tohoku Earthquake and a numerical modeling of the deformation of river embankments with a clayey subsoil layer," *Soils Found.*, vol. 52, no. 5, pp. 890–909, 2012, doi: 10.1016/j.sandf.2012.11.010.

[6] H. B. Seed and I. M. Idriss, "Simplified Procedure For Evaluating Soil Liquefaction Potential," *J. soil Mech. Found. Div.*, vol. 97, no. SM9, pp. 1249–1273, 1971.

[7] H. B. Seed, “Landslides during earthquakes due to soil liquefaction,” *J. Geotech. Eng.*, vol. 94, pp. 1055–1123, 1968.

[8] Y. Sasaki *et al.*, “Mechanism of permanent displacement of ground caused by seismic liquefaction,” *soils Found.*, vol. 32, no. 3, pp. 79–96, 1992.

[9] Y. Koga and O. Matsuo, “Shaking table tests of embankments resting on liquefiable sandy ground,” *Soils Found.*, vol. 30, no. 4, pp. 162–174, 1990.

[10] O. Matsuo, “Damage to river dikes,” *soils Found.*, vol. Special, pp. 235–240, 1996.

[11] M. Kitazume, *The Sand Compaction Pile Method*. 2005.

[12] K. Ishihara, Y. Kawase, and M. Nakajima, “Liquefaction characteristics of sand deposits at an oil tank site during the 1978 Miyagiken-oki earthquake,” *Soils Found.*, vol. 20, no. 2, pp. 97–111, 1980.

[13] K. Harada and J. Ohbayashi, “Development and improvement effectiveness of sand compaction pile method as a countermeasure against liquefaction,” *Soils Found.*, vol. 57, no. 6, pp. 980–987, 2017, doi: 10.1016/j.sandf.2017.08.025.

[14] H. Mitrani and S. P. G. Madabhushi, “Cementation liquefaction remediation for existing buildings,” *Gr. Improv.*, vol. 163, no. 2, pp. 81–94, 2010, doi: 10.1680/grim.2010.163.2.81.

[15] K. Adalier, A.-W. Elgamal, and G. R. Martin, “Foundation liquefaction countermeasures for earth embankments,” *J. Geotech. Geoenvironmental Eng.*, vol. 124, no. 6, pp. 500–517, 1998.

[16] M. Okamura and O. Matsuo, “Effects of remedial measures for mitigating embankment settlement due to foundation liquefaction,” *IJPMG-International J. Phys. Model. Geotech.*, vol. 2, pp. 1–12, 2002.

[17] M. Okamura and K. Tamura, “Prediction method for liquefaction-induced settlement of embankment with remedial measure by deep mixing method,” *soils Found.*, vol. 44, no. 4, pp. 53–65, 2004.

[18] A. Elgamal, E. Parra, Z. Yang, and K. Adalier, “Numerical analysis of embankment foundation liquefaction countermeasures,” *J. Earthq. Eng.*, vol. 6, no. 4, pp. 447–471, 2002.

[19] M. Kitazume, A. Takahashi, K. Harada, and N. Shinkawa, “New type sand compaction pile method for densification of liquefiable ground underneath existing structure,” *J. Geo-Engineering Sci. 3*, pp. 1–13, 2016, doi: 10.3233/JGS-150032.

[20] Y. Li, M. Kitazume, A. Takahashi, K. Harada, and J. Ohbayashi, “Dynamic FEM analyses on behavior of SCP improved ground with various geometry,” *Japanese Getechnical J.*, vol. 14, no. 2, pp. 161–178, 2019.

[21] M. Yoshida, M. Miyajima, and A. Numata, “Experimental Study on Liquefaction

Countermeasure Technique by Log Piling for Residential Houses," 2012.

[22] R. Rasouli, I. Towhata, and T. Akima, "Experimental Evaluation of Drainage Pipes as a Mitigation against Liquefaction-Induced Settlement of Structures," *J. Geotech. Geoenvironmental Eng.*, vol. 142, no. 9, p. 04016041, 2016, doi: 10.1016/j.jclinane.2008.08.024.

[23] R. Rasouli, I. Towhata, H. Rattez, and R. Vonaesch, "Mitigation of Nonuniform Settlement of Structures due to Seismic Liquefaction," *J. Geotech. Geoenvironmental Eng.*, vol. 144, no. 11, p. 04018079, 2018, doi: 10.1061/(ASCE)GT.1943-5606.0001974.

[24] J. Takemura, M. Kondoh, T. Esaki, M. Kouda, and O. Kusakabe, "Centrifuge model tests on double propped wall excavation in soft clay," *soils Found.*, vol. 39, no. 3, pp. 75–87, 1999.

[25] K. Harada and J. Ohbayashi, "Development and improvement effectiveness of sand compaction pile method as a countermeasure against liquefaction," *Soils Found.*, vol. 57, no. 6, pp. 980–987, 2017, doi: 10.1016/j.sandf.2017.08.025.

[26] G. Madabhushi, *Centrifuge modelling for civil engineering*. CRC Press, 2014.

[27] J. Osterberg, "Influence values for vertical stresses in semi-infinite mass due to embankment loading," in *Proceedings of the 4th international conference on soil mechanics and foundation engineering*, 1957, pp. 393–396.

[28] B. Mehrzad, Y. Jafarian, C. J. Lee, and A. H. Haddad, "Centrifuge study into the effect of liquefaction extent on permanent settlement and seismic response of shallow foundations," *Soils Found.*, vol. 58, no. 1, pp. 228–240, 2018, doi: 10.1016/j.sandf.2017.12.006.

[29] W. El-Sekelly, R. Dobry, T. Abdoun, and M. Ni, "Numerical Simulation of the Effect of High Confining Pressure on Drainage Behavior of Liquefiable Clean Sand," *J. Geotech. Geoenvironmental Eng.*, vol. 146, no. 12, p. 04020131, 2020, doi: 10.1061/(asce)gt.1943-5606.0002381.

[30] M. Ni, T. Abdoun, R. Dobry, K. Zehtab, A. Marr, and W. El-Sekelly, "Pore Pressure and Kσ Evaluation at High Overburden Pressure under Field Drainage Conditions. I: Centrifuge Experiments," *J. Geotech. Geoenvironmental Eng.*, vol. 146, no. 9, p. 04020088, 2020, doi: 10.1061/(asce)gt.1943-5606.0002303.

[31] T. Abdoun, M. Ni, R. Dobry, K. Zehtab, A. Marr, and W. El-Sekelly, "Pore Pressure and K σ Evaluation at High Overburden Pressure under Field Drainage Conditions. II: Additional Interpretation," *J. Geotech. Geoenvironmental Eng.*, vol. 146, no. 9, p. 04020089, 2020, doi: 10.1061/(ASCE)GT.1943-5606.0002302.

[32] S. Bhatnagar, S. Kumari, and V. A. Sawant, "Numerical Analysis of Earth Embankment Resting on Liquefiable Soil and Remedial Measures," *Int. J. Geomech.*, vol. 16, no. 1, p.

04015029, 2016, doi: 10.1061/(ASCE)GM.1943-5622.0000501.

[33] J. M. Pestana *et al.*, “Mechanisms of Seismically Induced Settlement of Buildings with Shallow Foundations on Liquefiable Soil Mechanisms of Seismically Induced Settlement of Buildings with Shallow Foundations on Liquefiable Soil,” *J. Geotech. Geoenvironmental Eng.*, vol. 136, no. 1, pp. 151–164, 2010, doi: 10.1061/(ASCE)GT.1943-5606.0000179.

[34] K. Kawasaki, T. Sakai, S. Yasuda, and M. Satoh, “Earthquake-induced settlement of an isolated footing for power transmission tower,” in *Centrifuge 98*, 1998, pp. 271–276.

[35] B. Ghosh, “Behaviour of Rigid Foundation in Layered Soils During Seismic Liquefaction,” *PhD thesis, Department of Engineering, University of Cambridge*. 2003.

[36] O. Adamidis and S. P. G. Madabhushi, “Deformation mechanisms under shallow foundations on liquefiable layers of varying thickness,” *Géotechnique*, pp. 1–12, 2017, doi: 10.1680/jgeot.17.P.067.

[37] M. Nasu, H. Fujisawa, and K. Hikimoto, “An experimental study on prevention of embankment deformation due to liquefaction of sandy ground,” *Q. Rep. Railw. Tech. Res. Inst.*, vol. 28, no. 1, pp. 5–6, 1987.

List of Tables

List of figures

Table 1 Summary of test conditions

Test code	Model description	Peak acceleration of input motion (gal)	
		First shaking	Second shaking
Case 1	Sand foundation without any improvement	150	220
Case 2	Vertical SCP improvement zone	140	210
Case 3	60 degrees SCP improvement zone	140	220
Case 4	50 degrees SCP improvement zone	140	240

Table 2 Index properties of Toyoura sand

Property	Value
Specific gravity, G_s	2.65
D_{50} (mm)	0.19
D_{10} (mm)	0.14
Maximum void ratio, e_{max}	0.973
Minimum void ratio, e_{min}	0.609
Permeability, k (m/s) at Dr=50%	2×10^{-4}
Permeability, k (m/s) at Dr=90%	1.5×10^{-5}

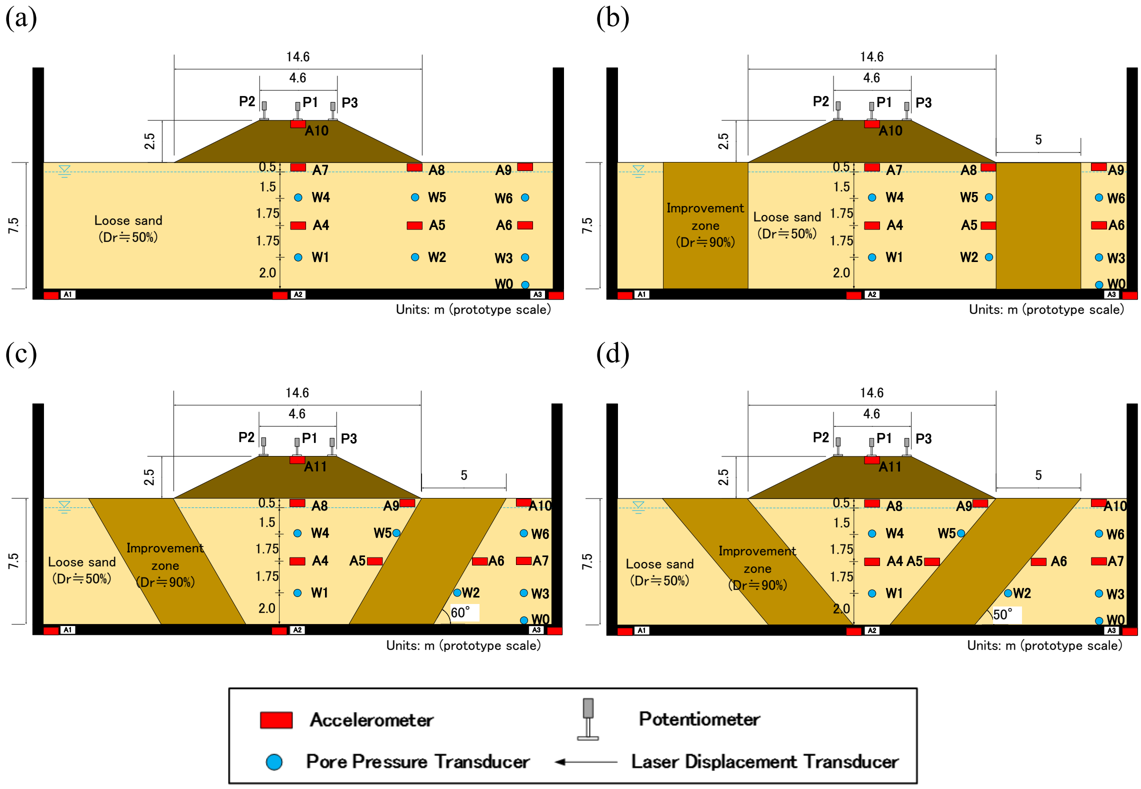

Fig. 1. Model configurations: (a) Case 1: unimproved ground, (b) Case 2: 90° improvement zones, (c) Case 3: 60° improvement zones, (d) Case 4: 50° improvement zones

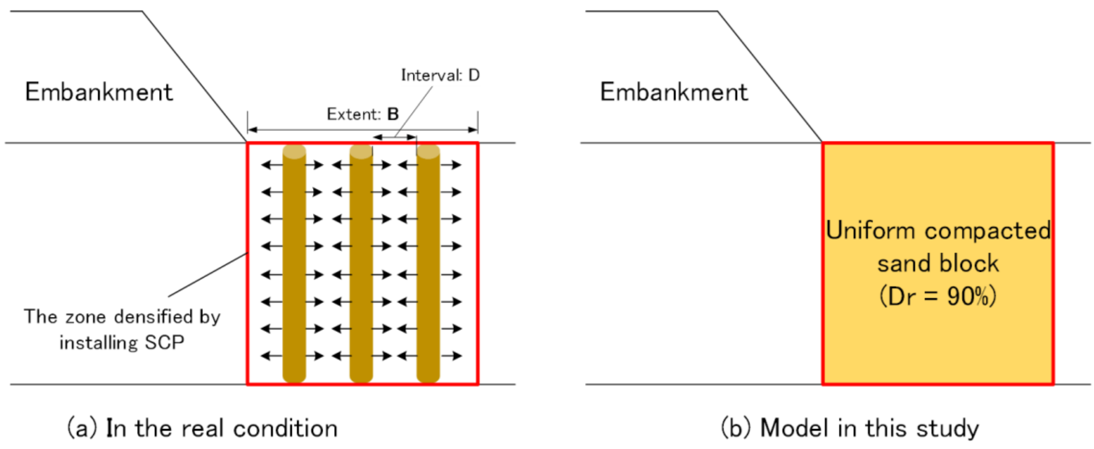

Fig. 2. Simplification of the SCP improvement zone modeled in the centrifuge experiment

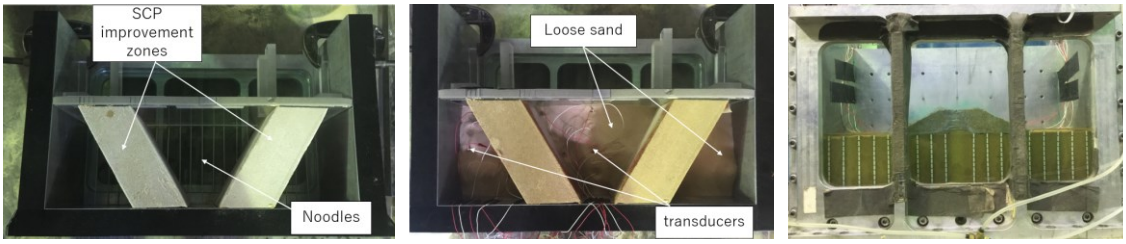

Fig. 3. Photographs of model ground preparation (Case 4)

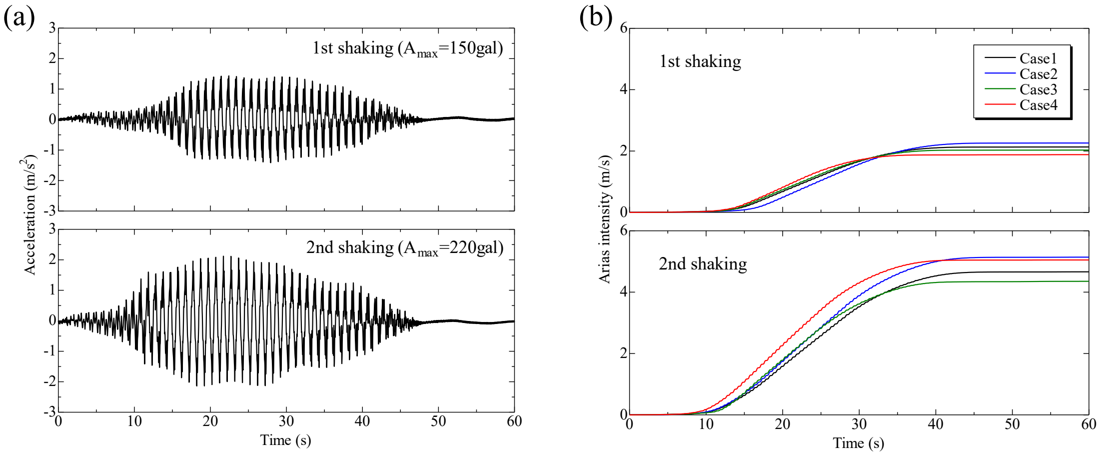

Fig. 4. (a) Acceleration time histories of input base motions for Case 1, (b) Arias intensities of input base shakings for all cases

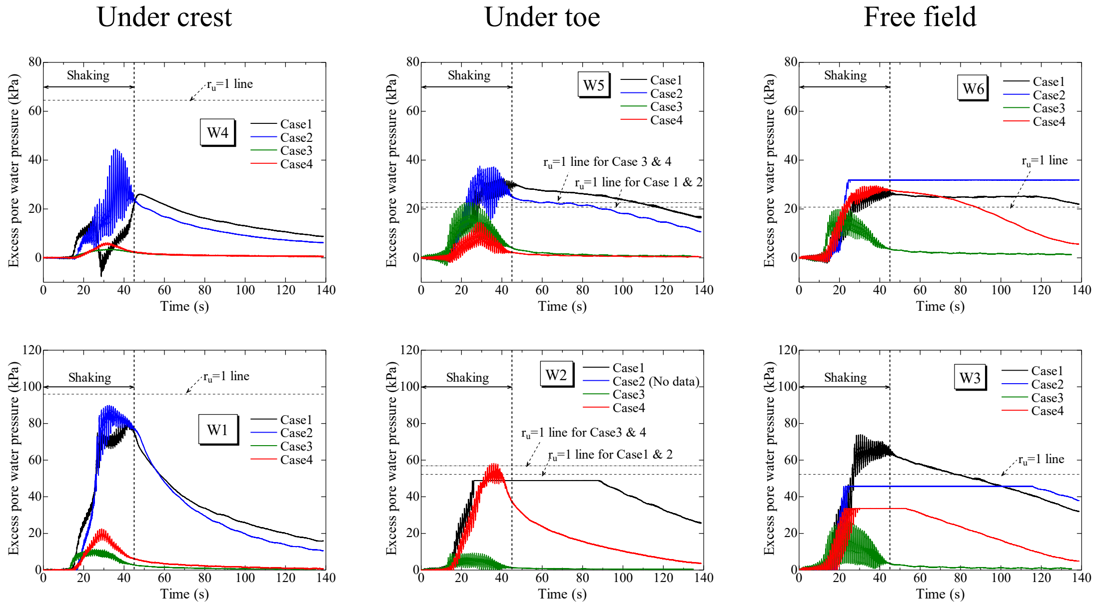

Fig. 5. Excess pore water pressure time histories during first shaking

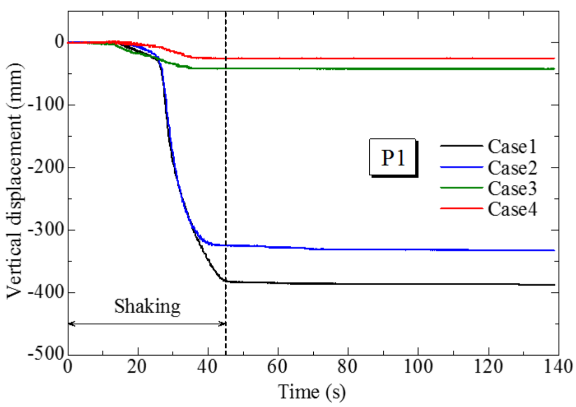

Fig. 6. Settlement time histories of the embankment crest during the first shaking

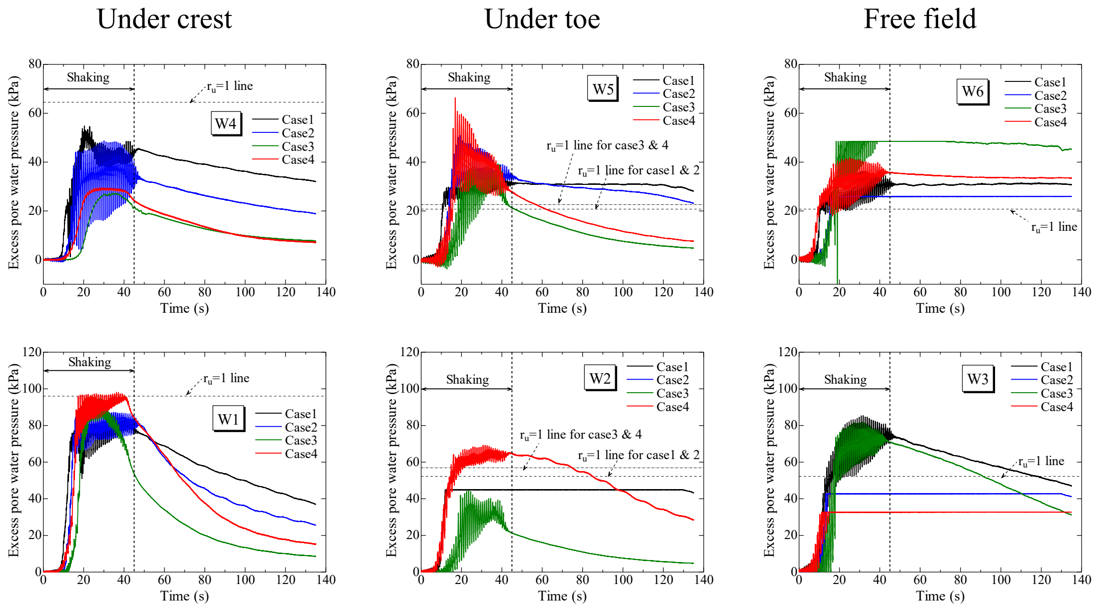

Fig. 7. Excess pore water pressure time histories during second shaking

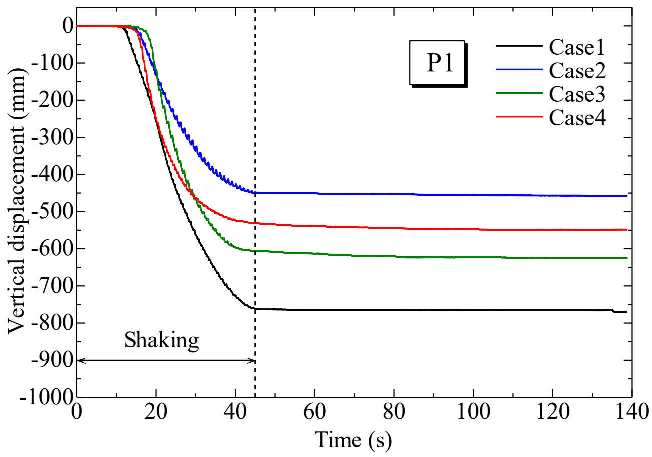

Fig. 8. Settlement time histories of the embankment crest during the second shaking

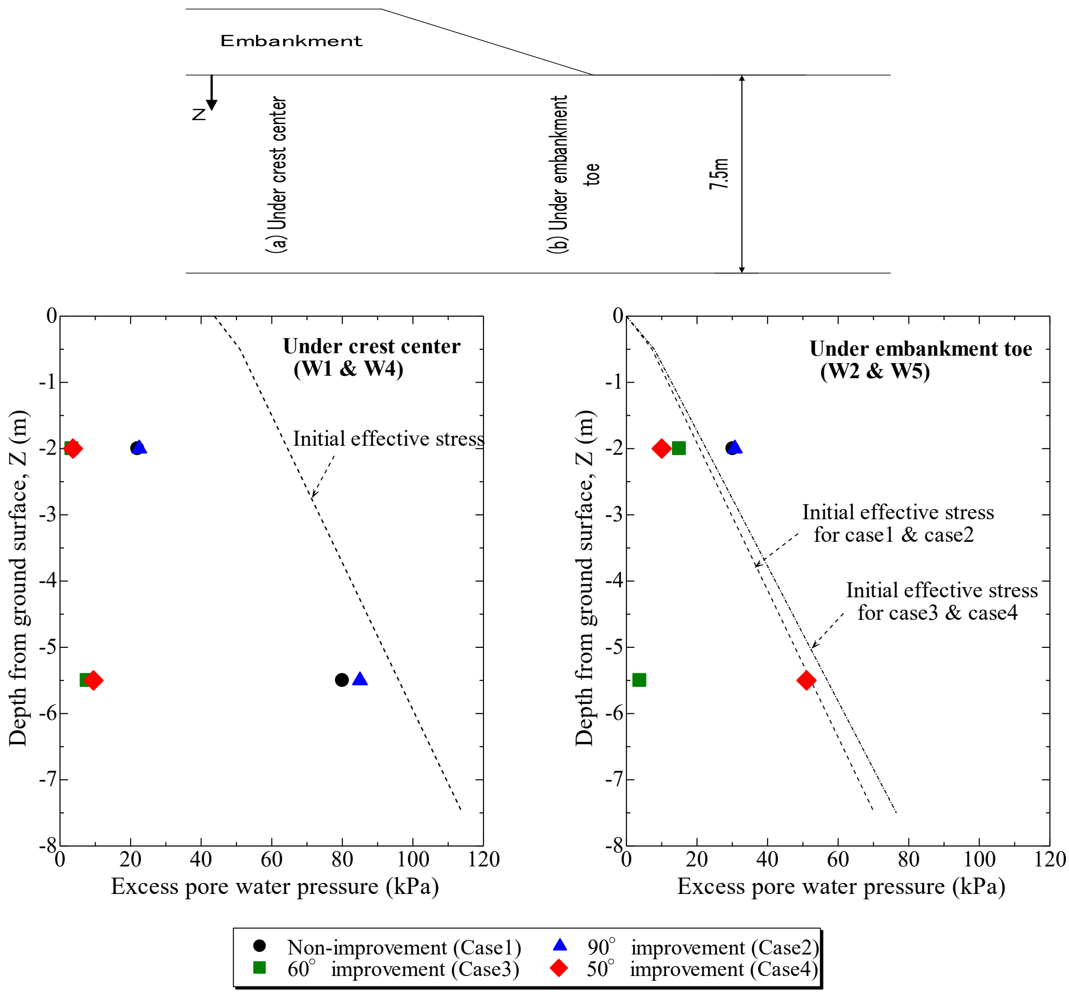

Fig. 9. Maximum excess pore pressure profiles during 1st shaking (A_{max}≈150 gal)

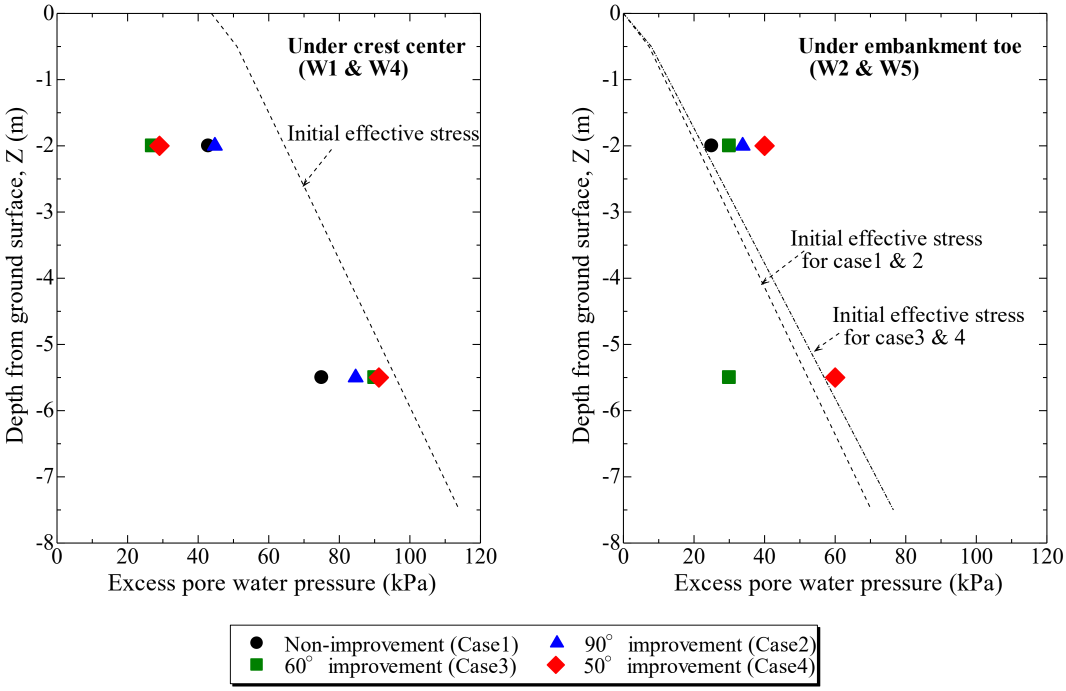

Fig. 10. Maximum excess pore pressure profiles during 2nd shaking (A_{max}≈220 gal)

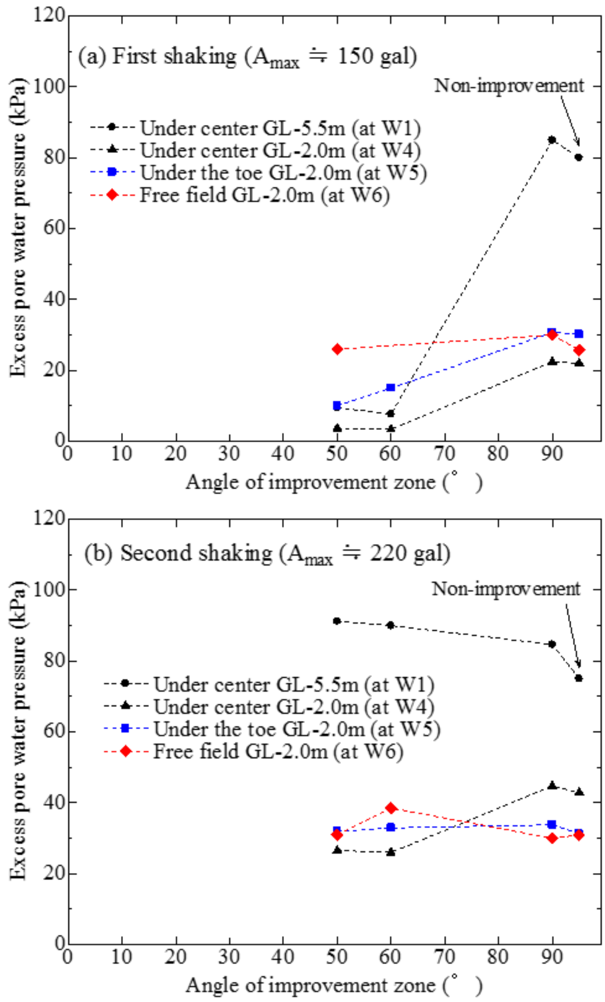

Fig. 11. Relationship between angle of improvement zone and maximum EPWP within the ground (at W1, W4, W5 and W6), (a) during first shaking, (b) during second shaking

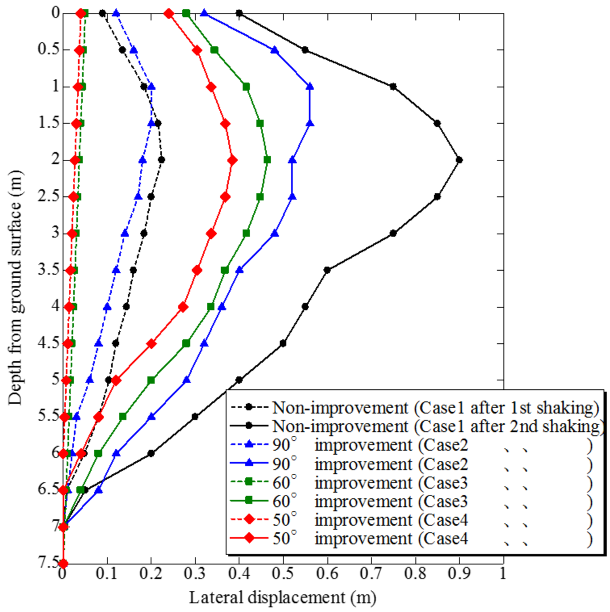

Fig. 12. Lateral displacement beneath the embankment toe (after first and second shaking)

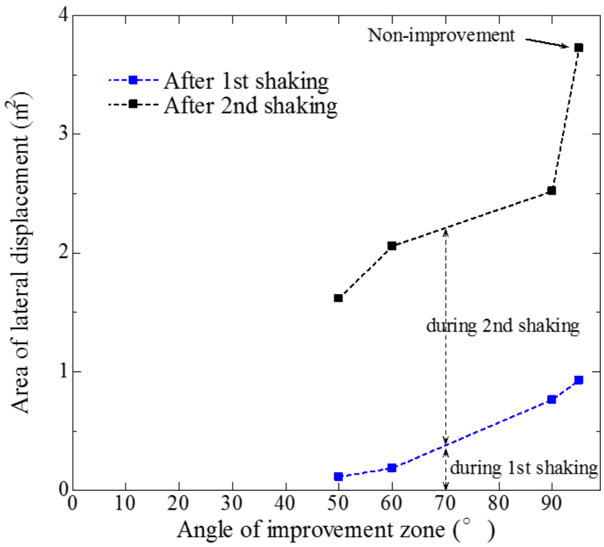

Fig. 13. Relationship between the angle of SCP remedial zone and area of lateral deformation

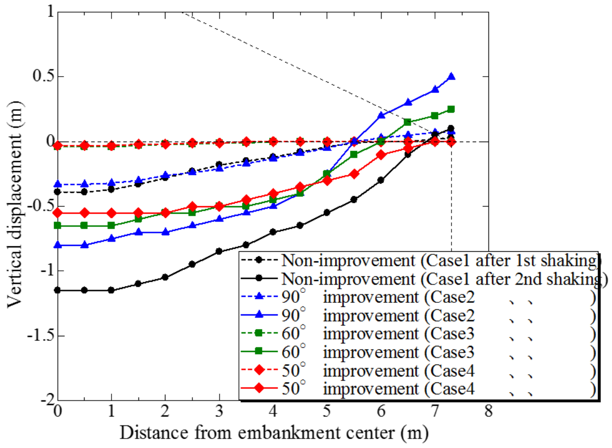

Fig. 14. Vertical displacement of the ground under embankment

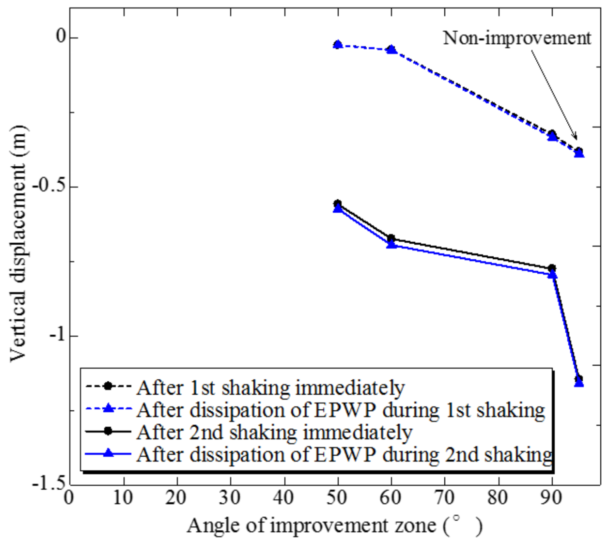

Fig. 15. Relationship between angle of SCP remedial zone and vertical displacement